Li *et al. Int J Concr Struct Mater* (2025) 19:11
https://doi.org/10.1186/s40069-024-00745-1

International Journal of Concrete Structures and Materials

RESEARCH

Open Access

Experimental Study on Repairing and Strengthening Seismically Damaged RC Frames by Installing H-Shaped Steel

Yuebing Li[1*], Qushenglin Song[1], Hang Wang[1], Liang Shan[2], Dawei Liu[3] and Shuang Xing[1]

Abstract

Seismic disaster investigations worldwide have revealed that a large number of reinforced concrete (RC) frame structures have been damaged or even collapsed. However, most of these buildings exhibit minor or moderate damage and can be repaired and strengthened. "Strong columns and weak beams, strong joints and weak components" is the concept of seismic design of buildings, and the failure of beam–column joints and columns is considered nonideal. For RC frame structures with damaged joints and columns, a method for repairing and strengthening damaged frames by installing *H*-shaped steel and pouring grout is proposed. By applying a pseudo static load, a frame structure specimen was damaged to simulate earthquake damage. After removing the crushed concrete, the damaged frame was repaired by pouring grout. Then, the structure was further strengthened by installing *H*-shaped steel on the columns using post-installed anchors. Through loading tests, seismic indices such as strength, deformation capacity, energy dissipation and failure mode of the frame before and after strengthening were compared. The results showed that the seismic performance of the repaired and strengthened frames exceeded that of the original frame, and the failure mode of the frame changed from joint shear and column-end bending to ideal beam-end yielding. Installing *H*-shaped steel and pouring grout could effectively strengthen the damaged frame, which provides a solution for repairing and upgrading damaged RC framed structures with a nonideal failure mode.

Keywords Frame structure, Joint failure, Reinforced concrete, Repairing and strengthening, Seismic damage, Structural steel installation

1 Introduction

Strong earthquakes cause the damage or collapse of a large number of buildings. Investigations on the 2008 Wenchuan earthquake showed that, except for a few areas with building collapse or serious damage, buildings in most of the affected areas were lightly or moderately damaged, belonging to the category of "repairable" (Wang et al., 2011), and 38% of them could be repaired and strengthened. From the point of view of the cost and urgency of solving people's living problems in disaster areas, it is more reasonable to carry out "repairing and strengthening" than "removing and rebuilding" for these kinds of buildings (Moeini et al., 2022). For earthquake-damaged buildings, "repairing" should not only ensure safety in normal cases, but also ensure that the buildings have sufficient seismic capacity in their subsequent working life (Cheng et al., 2024).

Reinforced construction (RC) frame structures are the most common structural form of buildings in China (Liu & Yang, 2020). The seismic code design concept

Journal information: ISSN 1976-0485 / eISSN 2234-1315.

*Correspondence:
Yuebing Li
sdlybing@hotmail.com
[1] School of Civil Engineering and Architecture, Northeast Electric Power University, Jilin 132012, China
[2] POWERCHINA Jilin Electric Power Engineering Co., Ltd., Changchun 130022, China
[3] Jilin Power Supply Company, State Grid Jilin Electric Power Company Co., Ltd., Jilin 132001, China

emphasizes "strong columns and weak beams, strong joints and weak members" (Han and Kang, 2023); therefore, beam-end bending failure in a frame structure under seismic action is the expected failure mode at the design stage. However, the formation of beam-end hinge mechanisms has seldom been observed in earthquakes in recent years, but a large number of joints or columns in frame structures have been damaged (Sanada et al., 2009, Shafaei et al., 2014). For post-earthquake repair and strengthening of damaged RC frame structures, researchers have proposed methods, such as increasing the cross section, pasting carbon fiber sheets (Islam et al., 2024), bonding steel, and adding bracing (Truong *et al.* 2017, Liuet al., 2023). However, these methods only aim at repairing and strengthening single members of beams, columns or joints, and no relevant research has been conducted on this nonideal damage form in which both beam–column joints and columns are severely damaged.

In this paper, for severely damaged RC frame structures at joints and columns, taking the beam-end yielding mechanism as the objective, a repair and strengthening method involving the combination of grout pouring and *H*-shaped steel installation is proposed. A 1/2-scale two-story, two-span RC frame was designed. Damage was generated to the RC frame by applying cyclic static loading to simulate a seismically damaged structure. Then, the frame was repaired by removing the severely crushed concrete and pouring grout into the parts where the concrete was removed. Moreover, the repaired frame was strengthened by installing *H*-shaped steel on the inner sides of the columns using post-installed anchors. The repaired and strengthened frame specimens were loaded again to verify the feasibility of the proposed method. By comparing the seismic performance of the structure before and after repair and strengthening, the strengthening effectiveness was analyzed. A solution is provided for the repair and strengthening of seismically damaged RC frame structures with nonideal damage modes.

2 Overview of Loading Tests

2.1 Specimen Design and Manufacture

Based on previous studies (Sashima et al., 2011, Sanada et al., 2013), a collapsed frame building in the 2009 Sumatra earthquake was taken as the prototype building to design the specimen. The building and details of the beam and column are shown in Fig. 1. In this building, severe damage, e.g., buckling of the column longitudinal reinforcement and core concrete crushing, was observed in the joints. The significant characteristics of the building are that instead of 135° hooks, the hoops in the beams and columns are 90° hooked, and the beam–column joint areas contain no hoops. A 1/2 scaled two-story, two-span specimen F is manufactured as shown in Fig. 2 (the frame

(a) View of the building and its damaged beam-column joint (Yasushi Sanada *et al* 2013)

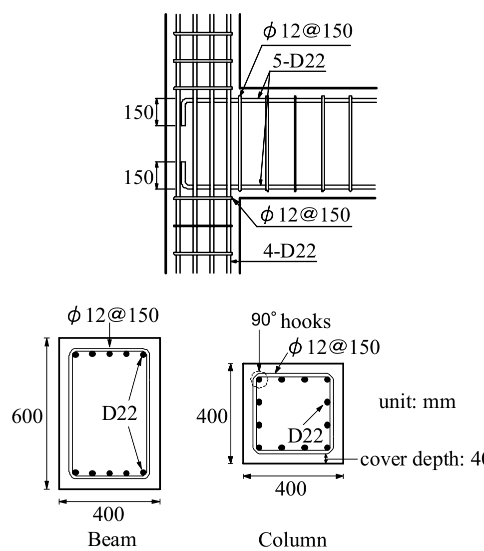

(b) Dimensions and reinforcement details of the studied exterior joint (Sashima Y *et al* 2011)

Fig. 1 View and details of the target building

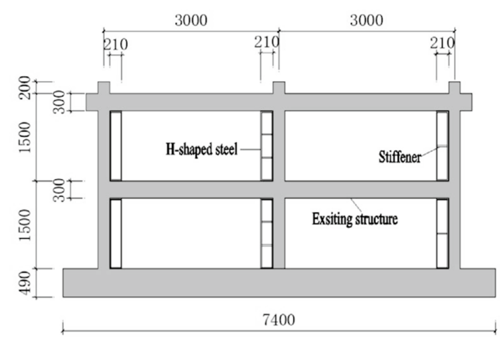

(a) Dimenions of the specimens (F/FR)

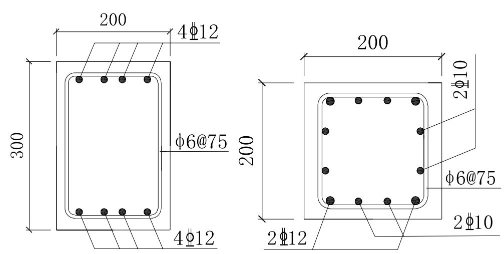

(b) Beam section (c) Column section

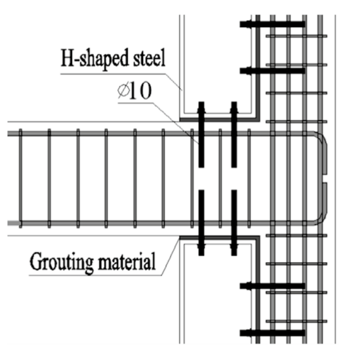

(d) Image of repaired and strengthened exterior joints

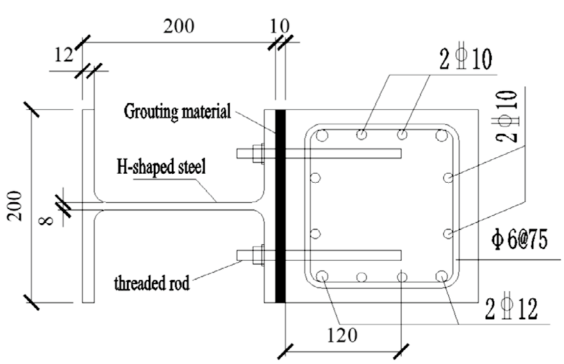

(e) Section of the repaired and strengthened columns

Fig. 2 Specimens

without *H*-shaped steel in the figure). The dimensions are shown in Fig. 2a, and the cross sections and reinforcement details of the beams and columns are shown in Fig. 2b and c. Similar to the prototypical building, and hooks for the hoop reinforcement in the beams and columns is 90°, and the joint area is not equipped with hoop reinforcement. The mechanical properties of the concrete and reinforcement used in the specimens are shown in Tables 1 and 2.

After it was subjected to cyclic static loads, specimen F, which was used for simulating a seismically damaged existing frame structure, was severely damaged and then repaired and strengthened, forming specimen FR (retrofitted frame), as shown in Fig. 1. The severely crushed concrete in specimen F was repaired using grout, as shown in Fig. 3, with the following steps: chipping away the crushed concrete with an electric hammer, cleaning the surface where the concrete was chipped with an air pump, installing the formwork for grout, wetting the interface of the existing concrete, mixing and pouring the grout, and then removing the formwork after 24 h curing. The grout used is a kind of high-strength nonshrinkage grout with a compressive strength of 54.6 MPa. Then, the repaired specimen was further strengthened by installing *H*-shaped steel with a size of $200\times200\times8\times12$ next to the existing columns. At the top and bottom of the *H*-shaped steel, a steel plate was welded for connection with the beams. As shown in Fig. 2a, horizontal stiffeners were welded in pairs on some of the *H*-shaped steels, with one pair for each steel adjacent to the right columns and two pairs for each steel adjacent to the middle columns, to study the effectiveness of the stiffeners on the strengthening effect.

Table 1 Mechanical properties of the concrete (MPa)

Design strength	Compressive strength	Tensile strength	Elastic modulus
C40	57.9	2.93	3.57×10^4

Table 2 Mechanical properties of the reinforcement and steel

Diameter (mm)	Specification	Yield stress (MPa)	Tensile strength (MPa)
6	HPB300	454.0	622.6
8	HRB400	464.8	684.6
10	HRB400	417.3	541.3
12	HRB400	479.0	623.0
10	Anchoring bar	324.9	452.0
–	*H*-shaped steel	263.2	426.0

(a) Damage to the exterior joint of specimen F

(b) Crushed concrete chipping

(c) Grout pouring

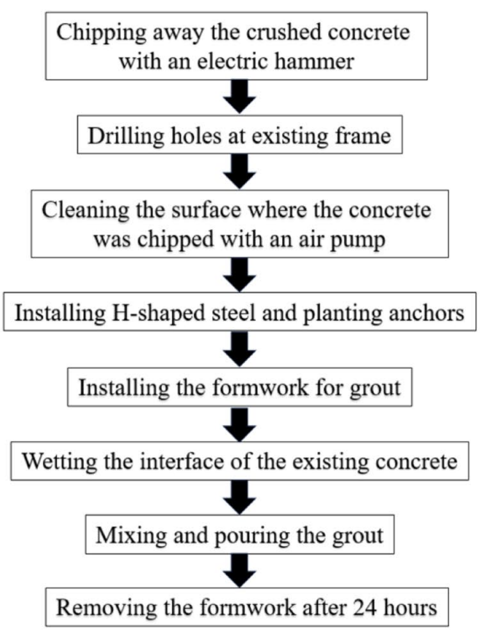

(d) Repair and strengthening process

Fig. 3 Repair and strengthening of the damaged of specimen F

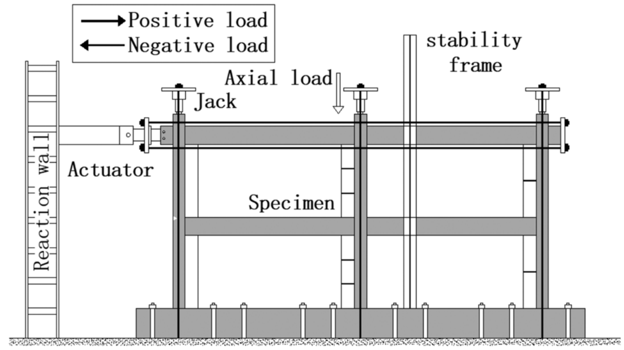

Fig. 4 Test setup

The *H*-shaped steels and the existing structure were connected by post-installed mechanical anchors, followed by wrapping with cement mortar, which were double-rowed at the column side and staggered at the beam side. The anchors were made of steel lead screws with a diameter of 10 mm. The embedded depth of the anchors in the existing structure was 12 d (d is the diameter of the reinforcement) by referring Li et al. (2019). A gap of 10 mm was reserved between the steel and the existing structure for pouring grout after the *H*-shaped steels were installed, as shown in Fig. 2d and e so that the steel and the existing frame could be closely connected to resist loads together. After repairing and strengthening, the existing part of the specimen was painted white again for easy observation of the cracks.

2.2 Test Setup and Loading Program

The test setup is shown in Fig. 4. The ground beam of the specimen is fixed to the stiff ground through high-strength steel rods, and a horizontal MTS hydraulic actuator is connected to the top beam of the specimen to apply cyclic static loads, defining the extending direction of the actuator as the positive loading and the contracting direction as the negative loading. Constant axial forces were applied to the columns using oil jacks, with an axial force ratio of 0.1 to the middle column and 0.05 to the side columns, which was the same as the prototype building.

The entire loading process was controlled by displacement, as shown in Fig. 5, with one cycle at each drift angle. The drift angle is defined as the ratio of the extended or contracted length of the actuator to its height from the top of the ground beam. Devices that clamped the specimen in front and behind were set for preventing out-of-plane displacement or collapse of the specimen. The loading was stopped when the strength of the specimen decreased to less than 85% of the maximum

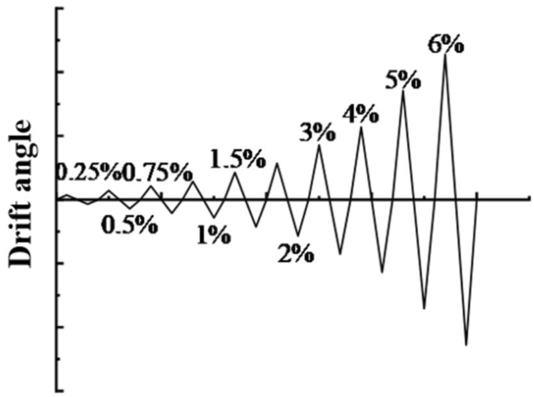

Fig. 5 Loading program

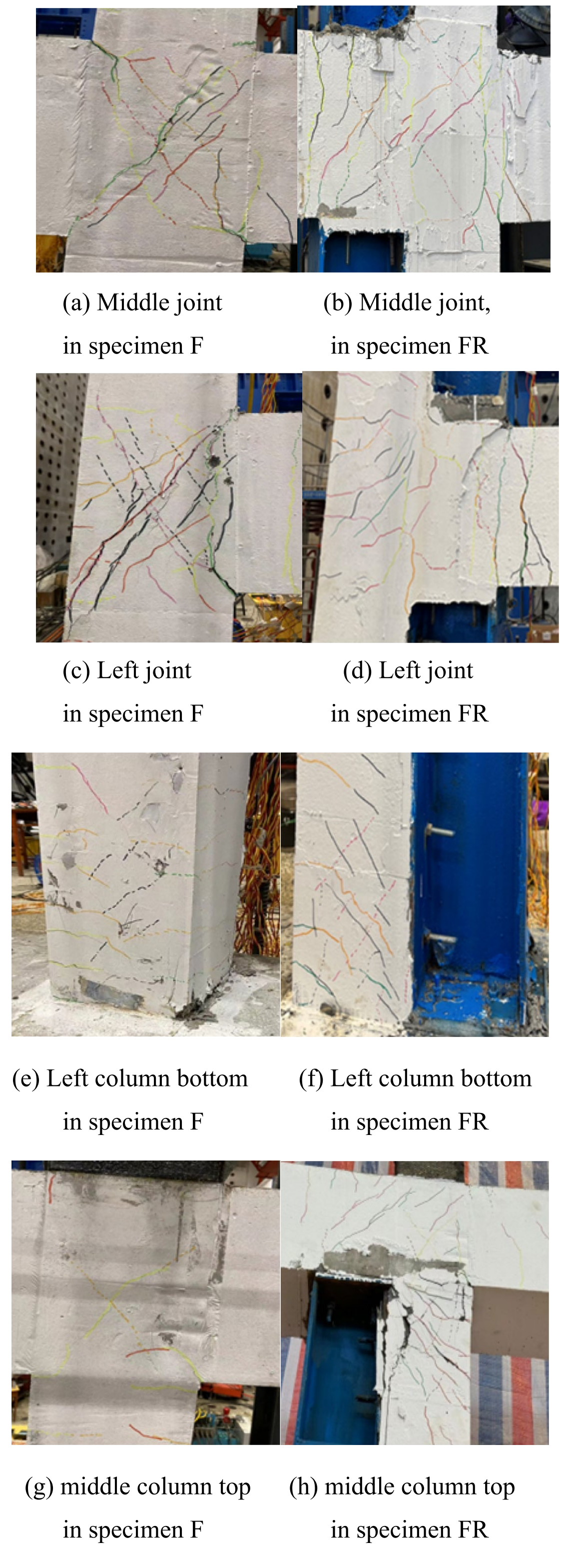

Fig. 6 Comparison of damage at each node of two specimens at maximum bearing capacity ($R = 3\%$)

value or when serious damage did not occur, preventing further loading.

2.3 Measurement

The strains of the longitudinal reinforcement at the critical sections of the beams and columns and the *H*-shaped steels at different height sections were measured using pasting strain gauges. Displacement transducers were arranged at the beam ends and joint areas of the first floor to measure the beam rotations and joint shear deformations. The concrete strain gauges were arranged diagonally in the joint area of the first floor. In addition, a crack width meter was utilized to measure the maximum crack width at important locations when loading to the peak displacement of each cycle.

3 Test Results

3.1 Experimental Phenomena

The crack patterns at the maximum strength ($R = 3\%$) of specimen F, which represents the seismically damaged frame, and specimen FR, which represents the repaired and strengthened frames, are shown in Fig. 6. The final crack patterns are shown in Fig. 7. The damage process is as follows.

Specimen F: As shown in Fig. 7a, the first floor was severely damaged at the bottom of the columns due to yielding of the longitudinal reinforcement and crushing and spalling of the concrete. The concrete in the joint area was crushed and spalled, and several cracks appeared at the beam ends, but the longitudinal reinforcement did not yield. The damage on the second floor was less severe than that on the first floor, and the most severe damage occurred at the top of the columns.

Specimen FR: The damage process of the repaired and strengthened specimens is highlighted. At a drift angle of $R = 0.25\%$, initial bending cracks appeared at the beam ends, and during positive loading, microcracks appeared

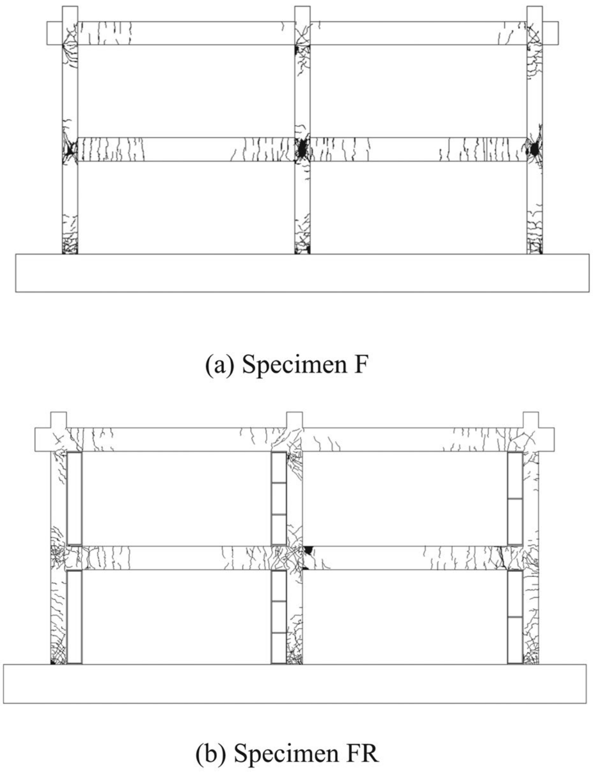

Fig. 7 Final crack patterns of the specimens

Fig. 8 End plate of *H*-shaped steel warping ($R = 1.0\%$)

between the boundary of the steel end plate and the grout at the bottom of the right and interior columns of the first floor. At $R = 0.5\%$, microdiagonal cracks appeared at the interior and right exterior joints of the second floor. At loading to $R = 0.75\%$, microdiagonal cracks appeared at the interior joint of the first floor, a few new bending cracks appeared at the bottom of the left and right columns, and new diagonal cracks appeared at the left exterior joint of the second floor. During the negative loading direction, the top end plate of the *H*-shaped steel at the left column of the second floor separated from the grout. When the loading reached $R = 1.0\%$, the diagonal cracks at the strengthened zone of the left beam end connecting the interior joint of the first floor expanded significantly, the bending cracks at the ends of the right beam widened significantly, and the bending cracks at the left column increased. During loading in the positive direction, the bottom end plate of the steel beside the interior column and the right column at the first floor were rotated approximately 2 mm apart, separating from the grout, as shown in Fig. 8. At $R = 1.5\%$, the diagonal cracks in the strengthened area where connecting steels at the left beam of the interior joint at the first floor further extended, the width of the bending cracks at the new critical section (at the location of the *H*-shaped steel face) increased to 1.6 mm, and concrete crushing occurred at the left end of the right beam and at the bottom of the interior column. At $R = 2\%$, the crack width at the boundary of the steel end plate of the right column of the first floor and the grout increased to 8 mm, and the concrete at the column bottom was slightly crushed. All the strengthening steels were well connected to the columns, the diagonal cracks at the joint area almost did not expand, and the cracks at the beam critical sections significantly expanded. At $R = 3\%$, the bending crack at the end of the right beam of the first floor expanded to 2.7 mm, and the grout under the bottom end plate beside the left column was crushed. The bottom end plates of the interior and right column warped considerably. The diagonal cracks at the interior joint of the second floor widened. The maximum strength was recorded in both the positive and negative loading directions, with the diagonal cracks in the exterior joints of the first floor almost not expanding. Moreover, no *H*-shaped steels yielded. At a drift angle of $R = 4\%$, the concrete at the bottom of the right column of the first floor was crushed, and bending deformation was observed at the *H*-shaped steel beside the left column. The diagonal cracks at the top of the left column of the second floor significantly widened. When the loading reached $R = 5.5\%$, at the bottom of the first floor of the interior column, the anchor bolt nuts connecting the end plate and the ground beam were pulled off, and the strength of the specimen decreased to 88.9% of the maximum value. Because the damage to the specimen was too severe, loading tests were stopped.

As shown in Fig. 7, the damage to the first floor of specimen F was mainly concentrated in the joints and bottom of the columns and concentrated in the top of the columns for the second floor. For specimen FR, the damage was mainly concentrated in the bottom of the columns, the interior joint, and the beam ends of the first floor. For

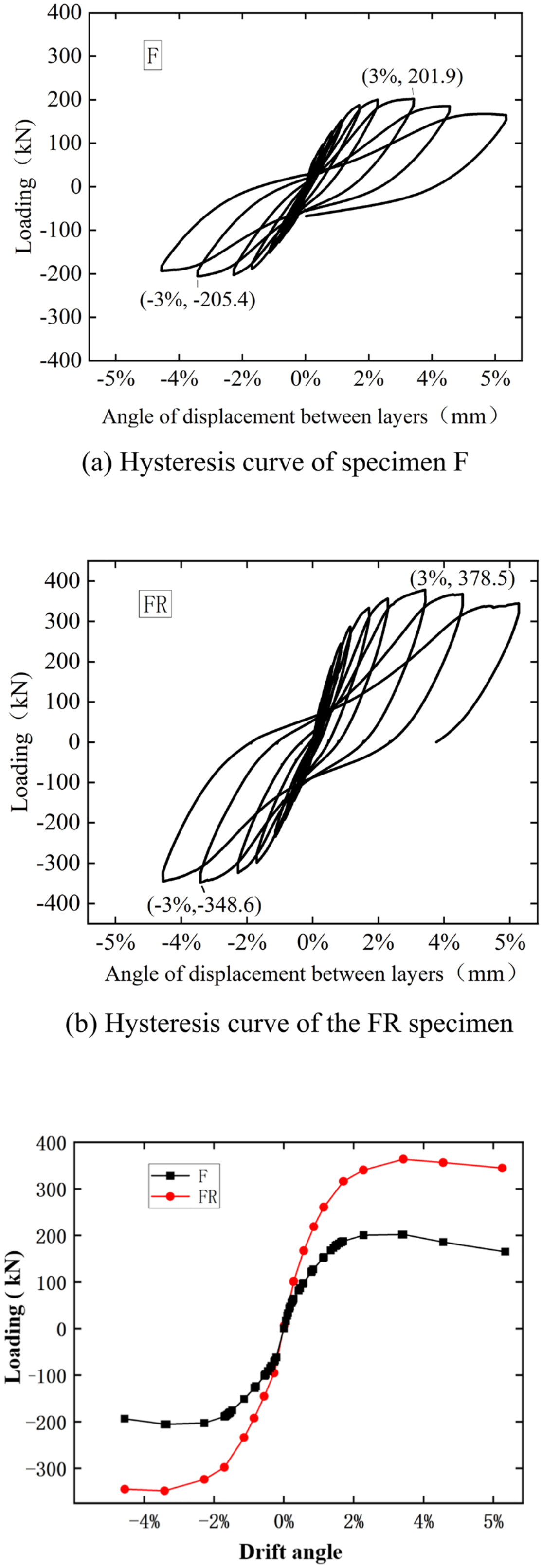

(a) Hysteresis curve of specimen F

(b) Hysteresis curve of the FR specimen

(c) Comparison of skeleton curves

Fig. 9 Load–displacement relationships and skeleton curves

the second floor, the damage was concentrated in the top of the interior column, the left end of the left beam, and the right end of the right beam. The connections between the *H*-shaped steel and the existing frame remained tight, and no significant buckling was observed on the steel. The grout did not separate from the existing concrete by maintaining intact bonding.

3.2 Hysteretic Behavior

The load–displacement relationship curves and the skeleton curves are shown in Fig. 9. Both specimens reached the maximum strength at a drift angle of 3.0%, and specimen F was + 201.9 kN and − 205.5 kN. FR was + 378.5 kN and − 348.6 kN in the positive and negative loading directions, respectively. After damaged specimen F was repaired and strengthened, the strength considerably improved by 87.5% and 69.6% in the positive and negative loading directions, respectively. The hysteresis curves of the FR specimen were plumper, and the strength decreased more slowly after reaching the maximum strength, indicating a better deformation capacity.

4 Analysis of Test Results

4.1 Stiffness Degradation

The stiffness degradation is evaluated by the secant stiffness *K* by Tiam shirzadi et al. (2024), which is the ratio of the sum of the absolute values of the positive and negative loads to the sum of the absolute values of the displacements at the peak in each loading cycle, as shown in Eq. (1):

$$K_i = \frac{|+F_i| + |-F_i|}{|+X_i| + |-X_i|}, \tag{1}$$

where + and − are the loading directions, F_i is the load at the peak of the *i*th loading cycle, and X_i is the displacement at the peak of the *i*th loading cycle.

The results are shown in Fig. 10. The stiffness of specimen FR is always greater than that of specimen F, and the stiffness of the structure significantly improved after repair and strengthening. At the beginning of loading, the stiffness of the two specimens degraded faster, and then the trend of stiffness degradation remained the same.

4.2 Energy Dissipation Characteristics

The area surrounded by one hysteresis loop was used to evaluate the energy dissipation capacity of the structure (Ninget al., 2014). A comparison of the cumulative energy dissipation Ea of the two specimens is shown in Fig. 11, which reveals that the energy dissipation capacity of the FR specimen was much greater than that of the F specimen.

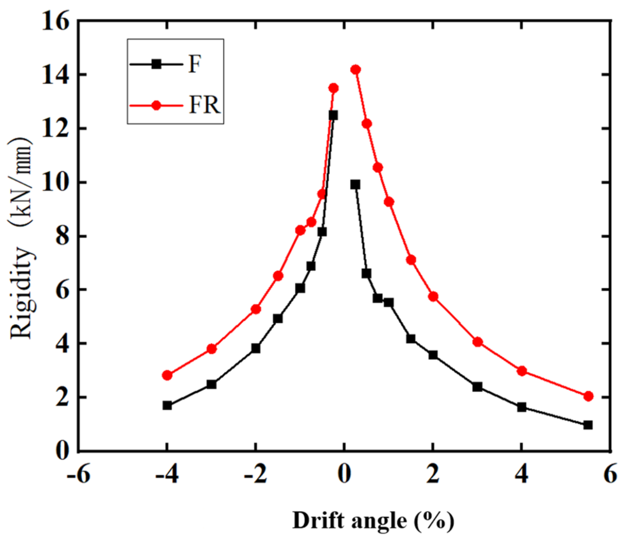

Fig. 10 Stiffness degradation

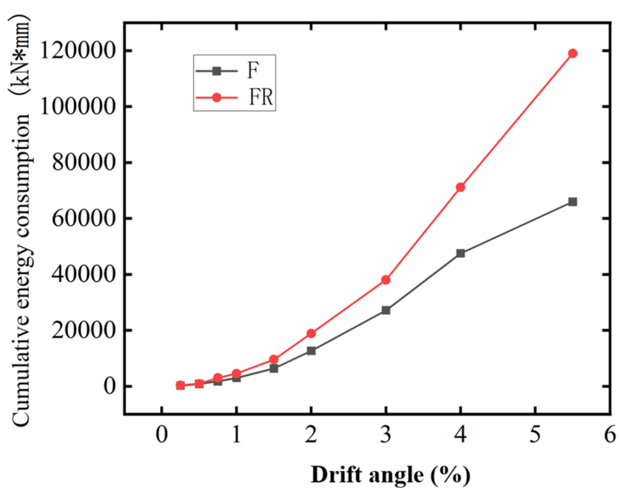

Fig. 11 Energy dissipation capacity

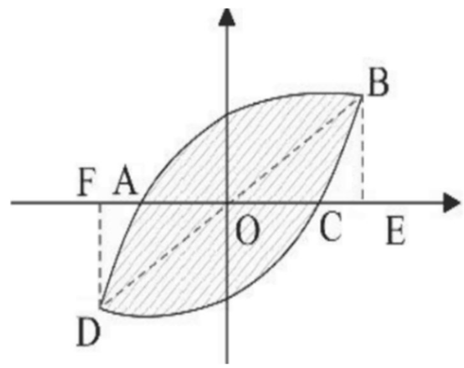

Fig. 12 Calculation diagram of the equivalent viscous damping coefficient

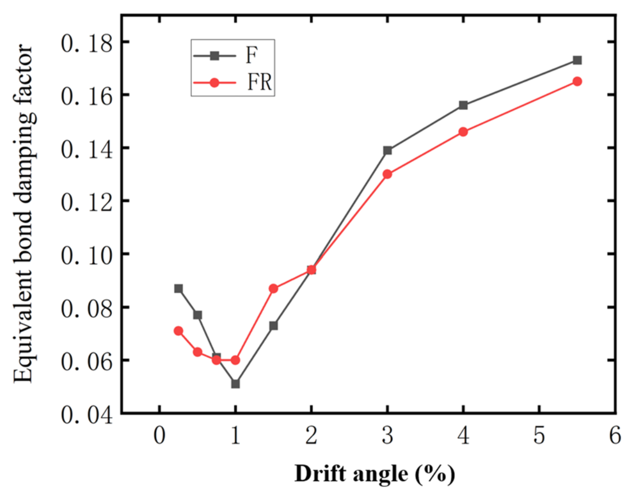

Fig. 13 Equivalent viscous damping coefficient

The equivalent viscous damping coefficient h_e (He, et al., 2023), which can be calculated via Eq. (2), reflects the energy dissipation efficiency of the structure. The calculation schematic and results are shown in Figs. 12 and 13, respectively. No large difference in the equivalent viscous damping coefficient was observed, showing that upon repairing and strengthening, the energy dissipation efficiency remained almost unchanged:

$$h_e = \frac{1}{2\pi}\frac{S_{(\mathrm{ABC+CDA})}}{S_{(\mathrm{OBE+ODF})}}, \tag{2}$$

where $S_{(ABC+CDA)}$ is the area of the hysteresis loop, and $S_{(OBE+ODF)}$ is the sum area of the two triangles, as shown in Fig. 11.

4.3 Joint Shear and Beam Bending Deformation

The joint shear deformation angle was calculated according to Eq. (3) using the data from the diagonally arranged displacement transducer in the joint area, as shown in Fig. 14. The results of the left exterior and interior joints at the first floor of the two specimens are shown in Fig. 15. As shown in Fig. 15a, the shear deformation at the exterior joint of specimen F barely increase in the early loading stage and increased rapidly in the later stage. For specimen FR, the value was always close to zero before $R = 3\%$ and increased slowly thereafter. Because the shear force applied to the interior joint in the loading process should be twice that applied to the exterior joint, Fig. 15b shows that the inhibitory effect of strengthening on the shear deformation of the interior joint was worse than that on the shear deformation of the exterior joint. However, the values of FR were still lower than those of F, and the inhibitory effect in the negative loading direction

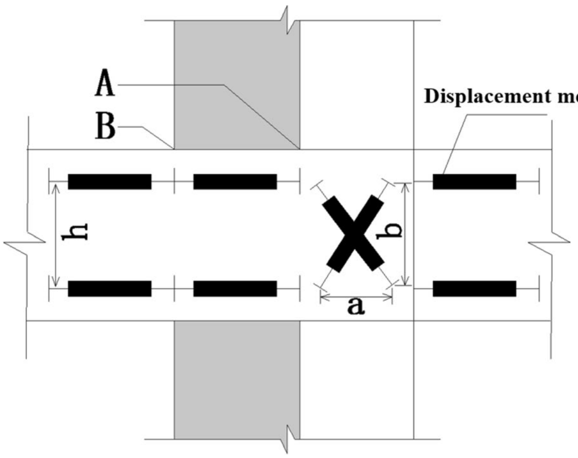

Fig. 14 Arrangement of the displacement transducers

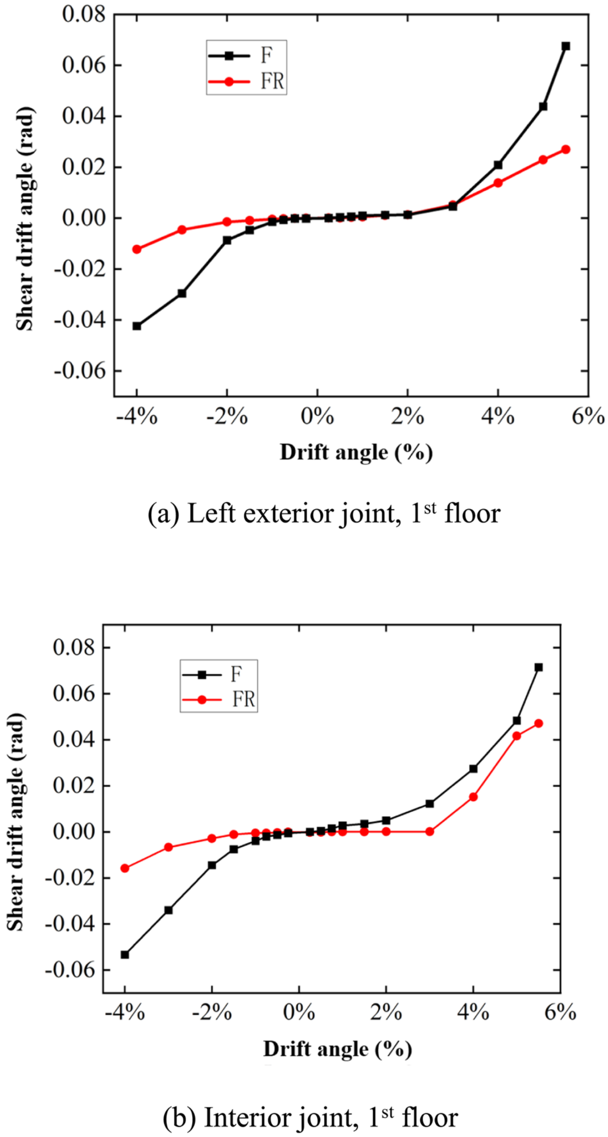

Fig. 15 Comparison on shear deformation of the joint on the first floor

was greater than that in the positive loading direction. Hence, in practical engineering strengthening, the strengthening design for interior joints needs to be emphasized, such as the selection of a larger steel section, to ensure the strengthening effect for interior joints:

$$\gamma = \frac{\sqrt{a^2 + b^2}}{\text{ab}}\left(\frac{\Delta_1 + \Delta_2}{2}\right), \tag{3}$$

where a and b are the side lengths of the measured area of the joint zone, as shown in Fig. 14, and Δ_1 and Δ_2 are the data obtained from the displacement transducers.

The rotation angle of the beams at the first floor was calculated based on Eq. (4) using the data measured by the displacement transducers arranged horizontally in pairs at the beam ends, as shown in Fig. 14. The results are shown in Fig. 16:

$$\theta = \frac{\Delta_1 + \Delta_2}{h}, \tag{4}$$

where Δ_1 and Δ_2 are the values measured by the upper and lower displacement transducers at the beam end, respectively, and h is the vertical spacing of the displacement transducers.

As shown in Fig. 16, the rotation angle at the critical section of the beam in specimen F, that is, at location A in Fig. 14, did not increase significantly with the loaded displacement, indicating that no plastic hinge was formed at the critical section of the beam. However, for specimen FR, the rotation angle at location B increased continuously with loading, indicating that the damage was concentrated in the new critical section of the beam and that a plastic hinge was formed after strengthening.

4.4 Strain of the Concrete at the Joint Region

The strains of the concrete at the interior and right joints of the first floor in specimen FR were measured using strain gauges. The strains are shown in Fig. 17, which are positive for tension and negative for compression. At a drift ratio of $R = 1.5\%$, the tensile strain at the right joint was 63,627 $\mu\varepsilon$, and at $R = 2\%$, the tensile strain at the interior joint area was 62,833 $\mu\varepsilon$, which was much greater than the ultimate tensile strain of the concrete (100 $\mu\varepsilon$). The maximum compressive strain of the concrete at the joint areas of the first floor did not exceed the ultimate compressive strain (3300 $\mu\varepsilon$), and the values were relatively small, indicating that the joint

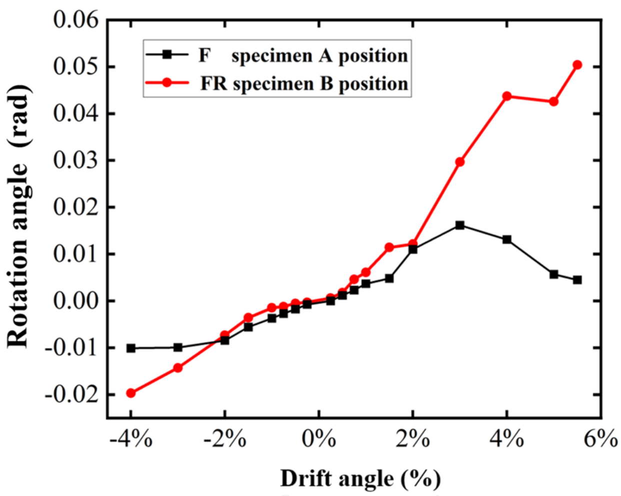

Fig. 16 Rotation angle at the left beam end connecting the middle joint on the first floor

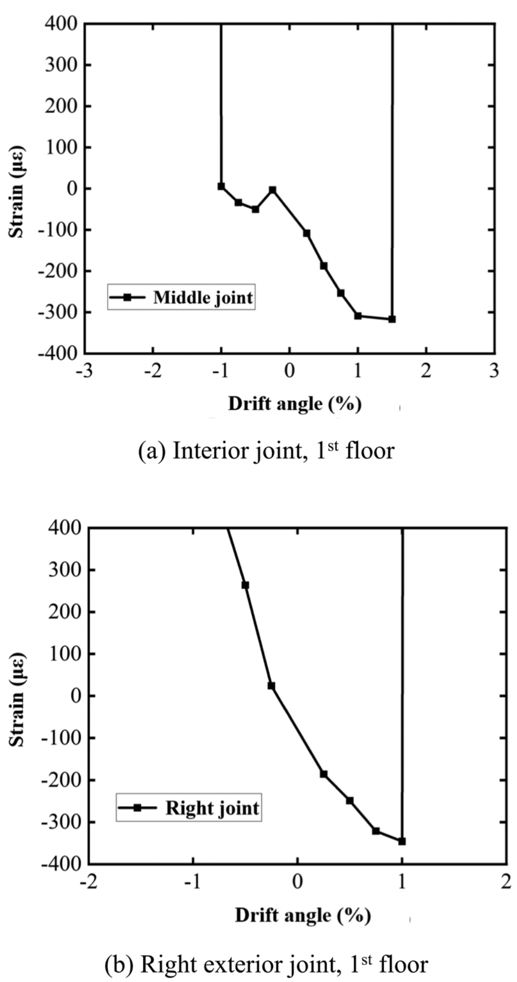

Fig. 17 Strain in the concrete at the joint regions

areas were effectively protected from shear failure after repair and strengthening.

4.5 Deformation Behavior

The deformation behavior of the structure was evaluated using the displacement ductility coefficient μ, which was calculated as shown in Eq. (5):

$$\mu = \frac{\Delta u}{\Delta y}, \tag{5}$$

where Δu and Δy indicate the ultimate and yield deformations of the specimen, respectively.

The yield deformation adopts an equivalent yield displacement, and the calculation method is shown in Fig. 18, connecting the origin and point A corresponding to $0.6P_u$ on the skeleton curve and extending to the line corresponding to P_u to intersect with point B. The displacement at point B is the yield displacement, which is shown as δ_y in the figure. The ultimate displacement is at point D on the skeleton curve when the strength decreases to 85%, which is shown as δ_u in the figure.

The ductility coefficient of specimen F was calculated to be 4.24. Since the strength of the repaired and strengthened FR specimen did not decrease to 85% when the loading tests were stopped but only to 89%, Δu was calculated to be 4.44 by using the displacement at the time when the strength decreased to 89%. Thus, the actual ductility coefficient of the FR should be above 4.44. The deformation capacity of the frame was improved by repair and strengthening.

4.6 Comparison of the Damage to the Left and Right Exterior Joints

As shown in Fig. 2a, the stiffeners were not arranged in the *H*-shaped steels connected to the left columns but

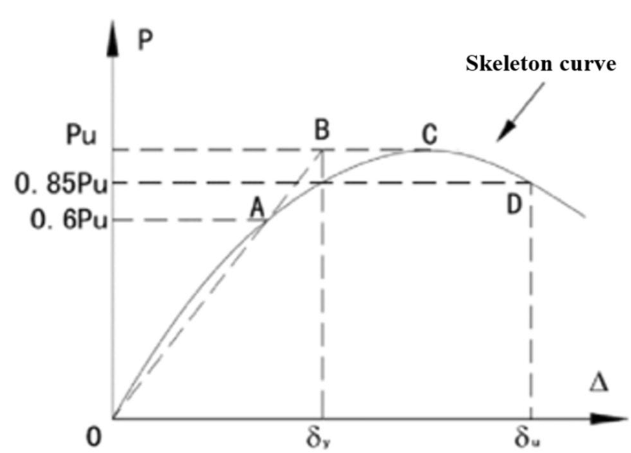

Fig. 18 Evaluation method of yield and ultimate displacement

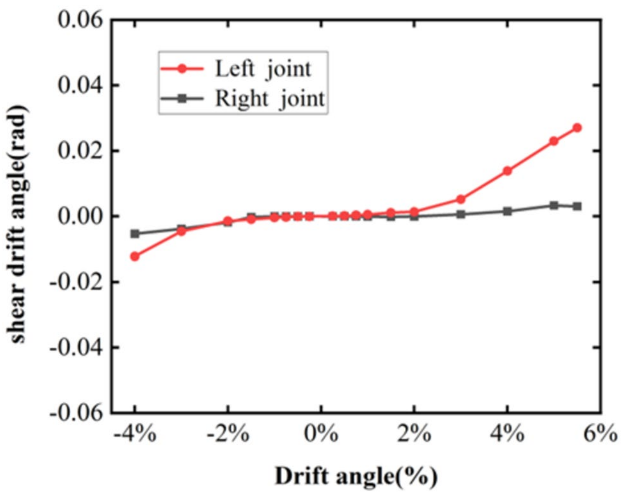

Fig. 19 Comparison of the shear deformation between the exterior joints on the 1st floor of the FR specimen

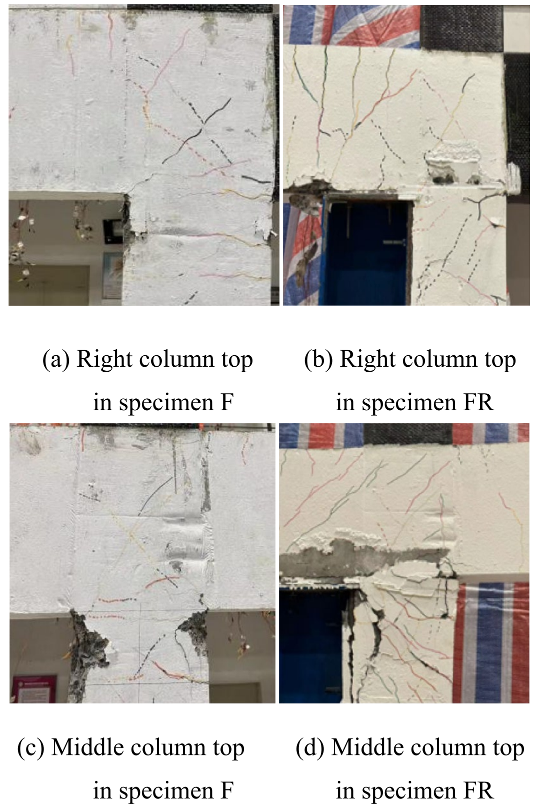

Fig. 20 Comparison of the final damage at the column top of the second floor

rather in the right columns, with the main purpose being to examine the necessity of arranging stiffeners. Fig. 19 compares the shear deformation of the left and right exterior joints at the first floor of specimen FR, illustrating that the shear deformation of the right joint where stiffeners were arranged in the *H*-shaped steel is smaller. Moreover, the test showed that the bending deformation of the steel adjacent to the right column was less than that of the other steels. Therefore, by arranging the stiffeners, the steel could achieve a better strengthening effect.

5 Analysis of Damage Patterns

The frame used to form an ideal beam-end bending failure mechanism was used for repair and strengthening. According to the damage phenomena of the structures and the deformation of the members, the failure patterns of the two specimens were determined to evaluate whether repair and strengthening were successful.

5.1 Second Floor

The final damage conditions of the areas around the right knee joint and interior *T*-shaped joint on the second floor of the two specimens are shown in Fig. 20. For the exterior knee joints in Fig. 20a and b, the damage to specimen F is concentrated at the column end where the concrete is crushed. The maximum crack of the FR specimen is located at the beam end, and the concrete is crushed. For the interior *T*-shaped joints, as shown in Fig. 20c and d, the tops of the columns in both specimens are severely damaged. The failure pattern at the top of the second floor of the frames can be determined as follows: for the exterior columns, plastic hinges were formed at the column top before strengthening and were transferred to the beam end after strengthening; for the interior column, plastic hinges were formed at the column top both before and after strengthening.

5.2 First Floor

Severe damage to the column bottom at the first floor of specimen FR was observed as shown in Fig. 21, with the concrete crushed and peeling off. However, the *H*-shaped steel did not yield as anticipated due to the warping of the bottom plate which was connected with the lower fixing stub as shown in Fig. 22. From the damage condition, it can be concluded that plastic hinges were formed at the column bottom of the first floor for the both specimens. All the joints at the first floor of specimen F were severely damaged by the formation of a joint hinge mechanism. After repair and strengthening, although many thin diagonal cracks appeared in the exterior joints of specimen FR, the main damage was concentrated in the beam ends, with concrete crushing, longitudinal reinforcement buckling, and the formation of plastic hinges at the beam ends. For the interior joint area, both the beam ends and the joint core area were severely damaged, but the joint damage was controlled considerably compared with that

(a) Left column bottom (b) Right column bottom

Fig. 21 Final damage to the bottom of the columns in specimen FR

(a)Left column bottom, at negative loading (b) Right column bottom, at positive loading

Fig. 22 *H*-steel warping at the bottom of the column at the first floor

of specimen F, and the plastic hinge mechanism occurred at the beam ends.

Overall, the plastic hinge positions of the structures are shown in Fig. 23. After repairing and strengthening, the first floor was transformed from joint hinging to beam-end hinging. At the second floor, column-end hinging was transformed to beam-end hinging for the exterior columns, and transformation of the plastic hinge at the interior column was not realized.

6 Conclusions

This study proposes a repair and strengthening method for seismically damaged frames, involving grout injection and the installation of *H*-shaped steel. By applying cyclic static loads to a simulated seismically damaged frame specimen and using the proposed repair method, the following main conclusions were drawn:

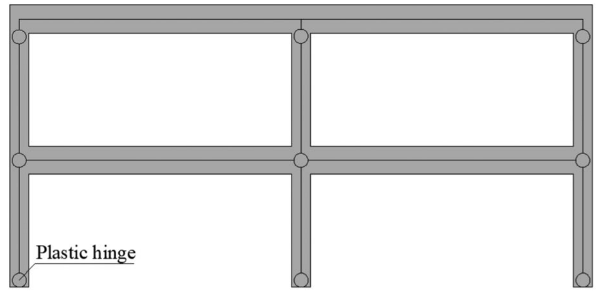

(a) Specimen F

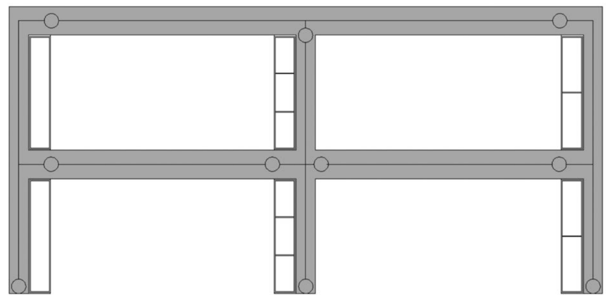

(b) Specimen FR

Fig. 23 Locations of the plastic hinges

- Significant improvement: the repaired and strengthened frame showed considerable improvements in strength, stiffness, energy dissipation, and ductility. Notably, it successfully avoided the joint-hinging mechanism and bending failure at the top of the exterior columns on the second floor.
- Beam-end hinging mechanism: after repair, the plastic hinge locations of the frame shifted from the joint locations to the beam ends, indicating that the strengthening effectively guided the location of plastic deformation, contributing to the overall performance of the structure.
- Control of interior joint damage: although the strengthening improved most damage situations, severe damage still occurred at the interior joints on the first floor, suggesting that further optimization of repair and strengthening for interior joints is needed.
- Effectiveness of grout and *H*-shaped steel: the post-poured grout maintained good bonding with the existing concrete, and the installation of *H*-shaped steel was securely connected with no significant yielding or deformation. However, during the later loading stages, nuts from the anchor bolts at the base of the column fell off, indicating that this aspect needs further improvement in future designs.

Acknowledgements
This research was financially supported by the International Science and Technology Cooperation Program of Scientific and Technological Developing Scheme of Jilin Province (Grant No. 20240402049GH) and the Research Foundation of the Education Department of Jilin Province (Grant No. JJKH20210101KJ).

Author contributions
All authors contributed to the study. Conception and design were performed by LI Yue-bing and XING Shuang. Material preparation, data collection and analysis were performed by SONG Qu-sheng-lin, WANG Hang, SHAN Liang and LIU Da-wei. The first draft of the manuscript was written by Song Qu-sheng-linand LI Yue-bing. All authors commented on previous versions of the manuscript. All authors read and approved the final manuscript.

Funding
This research was supported by the International Science and Technology Cooperation Program of Scientific and Technological Developing Scheme of Jilin Province, with the Grant No. 20240402049GH.

Availability of data and materials
The datasets used and/or analyzed during the current study are available from the corresponding author on reasonable request.

Declarations

Competing interests
The authors declare that they have no competing interests.

Received: 20 June 2024 Accepted: 3 November 2024
Published online: 07 February 2025

References

Ashtiani, F. A. D., & Farsangi, E. N. (2024). A novel Ductile Lightweight Fiber-Reinforced Concrete (DLFC) infill for seismic-prone zones: Experimental and numerical investigations. *Structures*. https://doi.org/10.1016/j.istruc.2024.106346

Cheng, S. T., He, H. X., Sun, H. D., & Cheng, Y. (2024). Rapid recovery strategy for seismic performance of seismic-damaged structures considering imperfect repair and seismic resilience. *Journal of Building Engineering*. https://doi.org/10.1016/j.jobe.2023.108422

Han, S. W., & Kang, H. (2023). Seismic behavior of high-performance fiber reinforced cementitious composites columns with limited reinforcement details. *Engineering Structures*. https://doi.org/10.1016/j.engstruct.2022.115419

He, W., Kang, J., Yang, S., et al. (2023). Experimental research on the seismic characteristics of a precast frame structure with a viscous damper. *Journal of Earthquake Engineering, 27*(4), 959–998.

Islam, N., Miyashita, T., & Ono, K. (2024). Repair of damaged composite girders using CFRP sheets considering limit state condition. *Journal of Constructional Steel Research*. https://doi.org/10.1016/j.jcsr.2024.108733

Li, Y. B., Sanada, Y., Maekawa, K., Katayama, H., Choi, H., Matsukawa, K., & Takahashi, S. (2019). Seismic strengthening and rehabilitation of RC frame structures with weak beam–column joints by installing wing walls. *Bulletin of Earthquake Engineering, 17*(5), 2533–2567. https://doi.org/10.1007/s10518-018-00547-3

Liu, R. Y., & Yang, Y. (2020). Experimental study on seismic performance of seismicdamaged RC frame retrofitted by prestressed steel strips. *Bulletin of EarthquakeEngineering, 18*(14), 6475–6486. https://doi.org/10.1007/s10518-020-00931-y

Liu, X., Zhang, J. W., Liu, J., Zhang, M., & Cao, W. L. (2023). Seismic performance and damage assessment of earthquake-damaged HSRAC columns with UHSS repaired by CFRP jackets. *Structures, 48*, 241–257. https://doi.org/10.1016/j.istruc.2022.12.078

Moeini, M. E., Razavi, S. A., Yekrangnia, M., Pourasgari, P., & Abbasian, N. (2022). Cyclic performance assessment of damaged unreinforced masonry walls repaired with steel mesh reinforced shotcrete. *Engineering Structures, 253*, 0141–0296. https://doi.org/10.1016/j.engstruct.2021.113747

Ning, N., Qu, W., & Zhu, P. (2014). Role of cast-in situ slabs in RC frames under low frequency cyclic load. *Engineering Structures, 59*, 28–38. https://doi.org/10.1016/j.engstruct.2013.09.050

Sanada, Y., Kishimoto, I., Kuroki, M., Sakashita, M., Choi, H., Tani, M. (2009). Preliminary Report on Damage to Buildings due to the September 2 and 30, 2009 Earthquakes in Indonesia. Proceedings of the Eleventh Taiwan-Korea-Japan Joint Seminar on Earthquake Engineering for Building Structures, Kyoto, Japan.

Sanada, Y., Tomonaga, T., Li, Y. & Watanabe, Y. (2013). Behavior of an R/C Exterior Beam–Column Joint without Concrete Confinement under Seismic Loading. *Proceedings of the Seventh International Conference on Concrete under Severe Conditions–Environment and Loading*, Vol. 2, pp. 1598–1606.

Sashima, Y., Nitta, Y., Tomonaga, T. & Sanada, Y. (2011). Seismic. Loading Test on an R/C Exterior Beam–Column Joint without Shear Reinforcements in Indonesia. *Proceedings of the Thirteenth Taiwan–Japan–Korea Joint Seminar on Earthquake Engineering for Building Structures*, Seoul, Korea, 68–77.

Shafaei, J., Hosseini, A., & Marefat, M. S. (2014). Seismic retrofit of external RC beam–column joints by joint enlargement using prestressed steel angles. *Engineering Structures, 81*, 265–288. https://doi.org/10.1016/j.engstruct.2014.10.006

Truong, G. T., Kim, J. C., & Choi, K. K. (2017). Seismic performance of reinforced concrete columns retrofitted by vari ous methods. *Engineering Structures, 134*, 217–235.

Wang, Q. L., Li, G. J., Liao, W. L., Zhang, L. F., & Qin, X. J. (2011). Building damages in Deyang city by the 2008 Wenchuan earthquake. *Geodesy and Geodynamics, 2*(4), 59–63. https://doi.org/10.3724/SP.J.1246.2011.00007.2

Publisher's Note

Yuebing Li Ph.D, Associate Professor, Mainly engaged in studies on seismic performance of concrete structures.

Qushenglin Song Master student, Mainly engaged in the study on repairing and strengthening of seismic damaged structures.

Hang Wang Master student, Mainly engaged in the study on seismic retrofitting of concrete frame structures.

Liang Shan Engineer, Mainly engaged in human resource management and structural design of industrial buildings.

Dawei Liu Engineer, Mainly engaged in project management on electric power engineering.

Shuang Xing Ph.D, Mainly engaged in studies on soil dynamics and frost heaving prevention of frozen soil.